Ali, M.; Ramirez Hoyos, P.; Duznovic, I.; Nasir, S.; Mafe, S.; Ensinger, W. (2017). Label-free histamine detection with nanofluidic diodes through metal ion displacement mechanism. Colloids and Surfaces B Biointerfaces. 150:201-208. doi:10.1016/j.colsurfb.2016.11.038

Label-free Histamine Detection with Nanofluidic Diodes through Metal Ion Displacement Mechanism

Mubarak Ali,[a,b]* Patricio Ramirez,[c] Ivana Duznovic,[a] Saima Nasir,[a] Salvador Mafe,[d] Wolfgang Ensinger[a,b]

[a]*Technische Universität Darmstadt, Fachbereich Material- u. Geowissenschaften, Fachgebiet Materialanalytik, Alarich-Weiss-Str. 2, D-64287 Darmstadt, Germany*

[b]*GSI Helmholtzzentrum für Schwerionenforschung, Planckstr. 1, D-64291 Darmstadt, Germany*

[c]*Departament de Física Aplicada, Universitat Politécnica de València, E-46022 València, Spain*

[d]*Departament de Física de la Tierra i Termodinàmica, Universitat de València, E-46100 Burjassot, Spain.*

*Corresponding author: E-mail address: M.Ali@gsi.de (M.Ali)

Abstract

We design and characterize a nanofluidic device for the label-free specific detection of histamine neurotransmitter based on a metal ion displacement mechanism. The sensor consists of an asymmetric polymer nanopore fabricated via ion track-etching technique. The nanopore sensor surface having metal–nitrilotriacetic (NTA–Ni^{2+}) chelates is obtained by covalent coupling of native carboxylic acid groups with N_{α},N_{α}-bis(carboxymethyl)-L-lysine (BCML), followed by exposure to Ni^{2+} ion solution. The BCML immobilization and subsequent Ni^{2+} ion complexation with NTA moieties change the surface charge concentration, which has a significant impact on the current–voltage (*I–V*) curve after chemical modification of the nanopore. The sensing mechanism is based on the displacement of the metal ion from the NTA–Ni^{2+} chelates. When the modified pore is exposed to histamine solution, the Ni^{2+} ion in NTA–Ni^{2+} chelate recognizes histamine through a metal ion coordination displacement process and formation of stable Ni-histamine complexes, leading to the regeneration of metal-free NTA groups on the pore surface, as shown in the current-voltage characteristics. Nanomolar concentrations of the histamine in the working electrolyte can be detected. On the contrary, other neurotransmitters such as glycine, serotonin, gamma-aminobutyric acid, and dopamine do not provoke significant changes in the nanopore electronic signal due to their inability to displace the metal ion and form a stable complex with Ni^{2+} ion. The nanofluidic sensor exhibits high sensitivity, specificity and reusability towards histamine detection and can then be used to monitor the concentration of biological important neurotransmitters.

Keywords: neurotransmitter; histamine; surface functionalization; nanofluidic sensor; NTA-metal complex.

1. Introduction

Neurotransmitters are considered as chemical messengers that transmit neurological information in the form of electrical signals within the cellular system of living organisms [1]. Up to date, more than 100 neurotransmitters have been identified by the scientists and are classified into different groups based on their chemical structures: i) biogenic amines (histamine, dopamine, serotonin, acetylcholine, etc.), ii) amino acids (glycine, glutamic acid, gamma-aminobutyric acid, etc.), iii) peptides (neurotensin, vasopressin, somatostatin, etc.), and iv) gaseous species (H_2S, NO and CO). A disturbance in the level of neurotransmitter content can adversely affect the transmission process, leading to depression, schizophrenia, drug dependence and degenerative diseases in human beings [2]. Histamine (Hm) naturally occurs in human body in trace amounts and plays a key role in physiological functions controlled by brain, for example, neurotransmission, sleep, memory storage, thermoregulation, inflammation, secretion of hormones and gastric acid, food intake and cardiovascular control [3-6]. An excess of Hm level in the body can cause Alzheimer's disease, abnormal arousal, asthma, allergies and some other neuropsychiatric disorders [7, 8]. Moreover, Hm is also present in some types of fish (e.g., tuna fish, sardine and mackerel, etc.) and cheeses where Hm concentrations ≥ 50 mg per 100 g can cause food poisoning [9, 10].

To date, different methods have already been developed for the detection of this biologically important amine, including gas chromatography [11], high-performance liquid chromatography (HPLC) [12, 13], capillary zone electrophoresis [14, 15], spectrofluorimetry [16-18], enzymatic assay [19], and flow immunoassay [20]. For example, Yamaguchi and co-workers have demonstrated selective and sensitive Hm sensing with HPLC coupled with fluorescence detection techniques [13]. Recently, Hm detection has been achieved via the modulation of fluorescence signals based on ligand exchange mechanisms using metal ion complexes [17, 18,

21]. To this end, Oshikawa *et al*. used a metal complex of cyanine dye for the determination of Hm released during the mast cell degranulation via a coordination displacement process [21]. Similarly, Seto *et al*. have also demonstrated the Hm detection based on specific coordination displacement between metal–iminodiacetic acid complexes and Hm analyte, leading to changes in fluorescence signal [17, 18]. The above techniques can be employed for the sensitive detection of various neurotransmitters but most of them need expensive instrumentation and are time consuming. It is of interest to design simple and low-cost detection techniques with fast response times and we demonstrate here a new label-free Hm detection method using a nanofluidic device.

During the recent years, asymmetric nanopores have been widely used for the miniaturization of (bio)chemical sensing devices because of their unique transport properties (e.g., permselectivity, gating, and current rectification) [22-27]. The sensing capability of these devices can be evidenced from the changes in the electronic read-out of the pore caused by the transport of an analyte under an applied voltage or the ligand-receptor interactions that occur upon the addition of analyte molecules in the bathing solutions. Previously, asymmetric nanopores have been successfully employed for the selective recognition of biomolecules [28-35], metal ions [36-41], anions [42-44], amino acid enantiomers [40, 45-49], and small organic molecules [37, 50]. However, there is still a room to expand the scope and potentialities of such tiny-sized pores by designing nanofluidic sensors for the detection of biogenic amines.

We present a nanofluidic sensing device for the label-free recognition of Hm. For this purpose, the pore surface is chemically decorated with nitrilotriacetic (NTA) moieties through the functionalization of N_{α},N_{α}-bis(carboxymethyl)-L-lysine (BCML) chains. Subsequently, the formation of NTA–Ni^{2+} chelates on the pore surface is achieved by exposing the BCML-modified pore to a Ni^{2+} ion solution. Upon metal ion complexation, the nanopore current-voltage

(*I–V*) characteristics are modified due to changes in the surface charge density. In the present case, the sensing principle is based on the displacement of Ni^{2+} from the NTA moieties. Due to the regeneration of NTA groups, the pore can be restored to the initial *I–V* characteristics. Among the various neurotransmitters examined in this study, only Hm is able to displace the metal ion from the NTA groups because of the formation of stable Ni-Hm complexes. The nanopore-based sensor exhibits high sensitivity, specificity and reusability towards Hm detection.

2. Materials and methods

2.1 Materials

The irradiation of 12 μm thick polyethylene terephthalate (PET) membranes (Hostaphan RN 12, Hoechst) was achieved at the linear accelerator UNILAC (GSI, Darmstadt) using single swift heavy ions (Au) of kinetic energy 11.4 MeV/nucleon.

All the chemicals and reagents were of analytical grade and used as received without further purification. *N*-(3-dimethylaminopropyl)-*N*-ethylcarbodiimide hydrochloride (EDC), pentafluorophenol (PFP), N_{α},N_{α}-bis(carboxymethyl)-L-lysine hydrate (BCML), glycine (Gly), serotonin (5-HT), gamma-aminobutyric acid (GABA), dopamine (DA) and histamine (Hm), sodium hydroxide and potassium chloride were purchased from Sigma-Aldrich, Schnelldorf, Germany.

2.2 Fabrication of single asymmetric nanopores

Before chemical etching of latent ion tracks, the swift heavy ion irradiated polymer membranes were sensitized with soft UV light. For this purpose, the tracked polymer membranes were exposed to UV irradiation on each side for 60 minutes. The UV sensitized latent ion damage tracks were converted into conical nanopores through the asymmetric track-etching technique

reported by Apel and co-workers [51]. The chemical track-etching process was performed in a custom-made conductivity cell having three chambers. This conductivity cell was employed for the simultaneous fabrication of single-pore and multipore membranes. To achieve this goal, a single-shot (1 ion hitting the foil) membrane and a membrane irradiated with 10^7 ions per cm^2 were placed on both sides of the middle compartment of the conductivity cell and clamped tightly. An etching solution (9 M NaOH) was filled in the middle compartment having apertures on both sides. In this way the chemical etchant was in direct contact with both the membranes. The two compartments on either side of the middle chamber were filled with a stopping solution (1 M KCl + 1 M HCOOH). To monitor the etching process, gold electrodes were inserted on both sides of the single-ion irradiated membrane and a potential of –1 V was applied across the membrane. The etching process was carried out at room temperature. The current remained zero as long as the etchant had not permeated the whole length of the membrane. After the breakthrough (a point at which the etchant pierced the membrane), an increase in the ionic current flowing through the nascent pore was observed. The etching process was stopped when the current reached a certain defined value. Then, the membranes were thoroughly washed with stopping solution in order to neutralize the etchant, followed by deionized water. The etched membranes were then dipped in deionized water overnight in order to remove the residual salts. This process resulted in polymer samples containing approximately conical single pores with carboxylic groups (COOH) generated on the inner pore walls due the hydrolysis of ester bonds in the back-bone of polymer chains.

2.3 Functionalization of nanopore surface

The COOH groups on the pore surface were first activated by exposing the single pore membrane to an ethanol solution of *N*-(3-dimethyl-aminopropyl)-*N*-ethylcarbodiimide (EDC; 100 mM) / pentafluorophenol (PFP; 200 mM) for 1 h at room temperature. A solution of N_{α},N_{α}-bis(carboxymethyl)-L-lysine hydrate (BCML) was prepared in an ethanol / water (8/2) mixture. The solution was neutralized by the addition of triethylamine. Then, the activated single pore membrane was exposed to BCML (25 mM) solution and the reaction was allowed to occur overnight. Finally, the functionalized membrane was washed several times with ethanol followed by deionized water.

2.5 NTA-Ni(II) complexation

For the complexation of Ni(II) ion with NTA moieties, a solution of $NiSO_4$ (100 mM) was prepared in deionized water. The pH of the $NiSO_4$ solution was adjusted to pH 10 with dilute NaOH. A polymer membrane containing a single BCML-modified pore was first washed with water (pH 10) in order to obtain fully ionized carboxylate groups. Then, the single pore membrane was immersed in a $NiSO_4$ solution for four hours at room temperature to achieve NTA–Ni(II) chelates on the pore surface.

2.6 Current-voltage measurements

The measurement of *I–V* curve was performed using a picoammeter/voltage source (Keithley 6487, Keithley Instruments, Cleveland, Ohio, USA) using LabVIEW 6.1 (National Instruments). For this purpose, the single-pore membrane (as-prepared and modified) was fixed between the two compartments of the conductivity cell. An aqueous electrolyte (100 mM) was filled in both halves of the cell. The Ag/AgCl electrodes were inserted into each half-cell solution to obtain a transmembrane potential and the ionic current flowing through the pore was measured. In the case of the conical nanopore, the ground and working electrodes were placed on

the base and tip side of the pore, respectively. In order to record the *I–V* curves, a scanning triangle voltage signal from −1 to +1 V was used.

2.7 Theoretical modeling

The experimental *I–V* curves were analysed in terms of a simplified, one dimensional (1D) theoretical model based on the Poisson-Nernst-Planck (PNP) equations [52-54]. Assuming a conical geometry, the unknown model parameters are the tip (d), base (D) diameters of the pore and the surface charge density (σ). These parameters can be determined independently following a protocol established previously [52-54]. Briefly, the diameter of the pore base was estimated by microscopy techniques using polymer samples containing 10^7 pores per cm^2 which were etched simultaneously with the single pore samples used in the experiments. The diameter of the pore tip was calculated from the slope of the *I–V* curve measured with 1 M KCl solution at low applied voltages. Under these conditions, the Dukhin number (σ over the product of the salt concentration and pore radius, see reference [55] becomes small and the nanopore shows to a quasi-linear *I–V* curve. Once the pore diameters had been calculated, the surface charge density in each experiment was determined by fitting the theoretical model to the experimental data.

3. Results and discussion

The COOH groups generated on the pore surface serve as the starting point to modulate chemical characteristics of the nanopore as well as dictate the surface charge and permselectivity. Under physiological conditions, the as-prepared conical pore preferentially transports cations due to the ionization of carboxylate groups, resulting in *I–V* curves similar to that of biological ion channels [52-54, 56-58]. The nanopore surface properties and ion transport characteristics can be modulated through the appropriate chemical functionalization. In the present case, the transport

behavior of the single conical pore was tuned through NTA functionalization and the concomitant formation of metal chelates on the surface.

Figure 1 shows the chemical reaction scheme followed to tune the chemical characteristics of the pore surface. The immobilization of BCML chains having NTA moieties is achieved through carbodiimide coupling chemistry. For this purpose, the COOH groups are first activated into amine-reactive molecules by exposing the single pore membrane to *N*-(3-dimethylaminopropyl)-*N*′-ethylcarbodiimide (EDC) and *N*- pentafluorophenol (PFP) solution. Then, the PFP-reactive intermediates are further covalently coupled with the amine group of BCML molecules. After BCLM functionalization, the next step is to prepare the metal chelates on the surface. To achieve this goal, the pore decorated with NTA moieties is exposed to an alkaline solution containing Ni^{2+} ions. The BCML functionalization and subsequent NTA–Ni^{2+} complexation are confirmed by measuring the *I–V* curves.

Figure 2(A) shows the *I–V* characteristics of the single conical pore with COOH groups, NTA moieties and NTA–Ni^{2+} chelates on the pore surface, respectively. Note that a single pore membrane remained fixed in the conductivity cell in each case. After each functionalization step, the reactant solution is replaced with the working electrolyte (100 mM KCl) solution for the measurement of the *I–V* characteristics. The ground electrode is placed on the base side, while the working electrode is fixed on the tip opening side, serving as a cathode for positive bias and an anode for reversed bias. In this electrode configuration, high (> 0 nA) and low (< 0 nA) ionic currents are recorded for the positive and negative voltages, respectively. The as-prepared pore exhibits current rectification (cations preferentially flows from the tip opening towards the base opening) due to the existence of ionized carboxylate (COO^{-}) groups which impart negative charge to the pore surface [52-54, 56-58].

BCML immobilization produces significant changes on the *I–V* characteristics of the modified nanopore, compared to the as-prepared nanopore because of the increase in the number of negative fixed charges [33]. This process yields an increase of the pore conductance *G* at positive applied voltage. Exposing the BCML-modified pore to a Ni^{2+} ion solution gives a decrease of the pore conductance, as evidenced from the *I–V* characteristics. On the formation of NTA–Ni^{2+} chelates, most of the NTA carboxylate (COO^{-}) groups are neutralized due to Ni^{2+} ion complexation, which in turn diminishes the surface charge density. This fact clearly shows the successful immobilization of BCML chains having NTA moieties and concomitant NTA–Ni^{2+} complexation on the nanopore surface. The pore conductance is then correlated with the surface charge density and can be quantified by its value at 1 V, *G*(1 V). Figure 2(B) shows the values of *G*(1 V) obtained from the corresponding *I*−*V* curves. After decorating NTA moieties on the pore surface, *G*(1 V) increases from 3.9 nS to 4.9 nS due to the increase of the fixed charge density. Upon Ni^{2+} ion complexation with NTA groups, *G*(1 V) decreases to 2.7 nS, suggesting the loss of pore surface charge.

In the next step, the NTA–Ni^{2+} chelated pore is successfully employed as a sensing device for the selective recognition of neurotransmitters. To this end, Hm is chosen as a model neurotransmitter. Hm contains a primary amino group, a secondary imidazole nitrogen and a tertiary imidazole nitrogen atom. The secondary nitrogen does not take part in coordination reaction. Hm is then considered as a bidentate ligand and makes a six membered ring with metal ion [59-61]. For the control experiment, various neurotransmitters including glycine (Gly), serotonin (5-HT), gamma-aminobutyric acid (GABA) and dopamine (DA) are employed. An aqueous KCl (100 mM, pH 7.1) solution is used to prepare the analyte concentrations.

Note that the ionic transport through the nanopore is mainly governed by three mechanisms: (i) volume exclusion (partial/complete pore occlusion), hydrophobic/hydrophilic interactions

(changes in pore wettability), and electrostatic interactions (changes in the surface charge). In the present case, we consider the electrostatic interactions: the sensing process leads to changes in the magnitude of fixed surface charges via the complexation/decomplexation of Ni^{2+} ion with the NTA in the nanoconfined environment.

Figure 2(C) and 2(D) show, respectively, the *I–V* curves for positive applied voltage and the resulting *G*(1 V) values obtained upon exposing the NTA–Ni^{2+} chelated pore to the working electrolyte with a 1 mM concentration of various neurotransmitters, separately. The presence of Gly and 5-HT in the electrolyte solution in contact with the NTA–Ni^{2+} chelated pore induce minor changes in *G*(1 V). This fact confirms their inability to displace complexed Ni ions from the chelates, leaving the original sensor surface undisturbed. For the case of GABA and DA, the increases in *G*(1 V) are comparatively higher. These results suggest a partial removal of chelated Ni^{2+} ions only, while most of the NTA–Ni^{2+} complexes still remaining on the pore surface. Upon exposure to Hm solution, however, the metal ion chelated pore exhibits a clear increase in *G*(1 V), similarly to the modified pore. The displacement of metal ions from the NTA–Ni^{2+} chelates by Hm leads to the formation of Ni-Hm complexes [17, 18, 21]. Eventually, the exposed metal-free NTA groups boosts the surface charge density, giving an increase in the forward current at positive potential, which suggest that only Hm is able to displace the metal ion to a large extent from the NTA moieties. This occurs because of the presence of the imidazole and amino groups in close proximity, which results in the formation of stable six membered ring chelates $[Ni(Hm)_3X_2]$ compared to the other neurotransmitters examined here [17, 18, 21].

The continuous lines in Figures 2(A) and 2(B) show the theoretical *I–V* curves obtained with the effective 1D model. The diameters of the pore and the concentration of fixed charges were determined using the procedure described in section 2.7. The surface charge density in each experiment was obtained from the best fitting at $V = 1$ V. The theoretical curves follow the

experiments. In particular, the model results of Figure 2(A) account for the increase of G(1 V) after BCML immobilization, when compared to the as-prepared nanopore, because of the increase of σ due to the presence of NTA moieties. The conductance decrease obtained after exposition of the modified pore to a Ni^{2+} ion solution is due to the neutralization of the fixed charges. The theoretical curves of Figure 2(C) allow for the estimation of the concentration of fixed charges in the pore walls after the exposition of the NTA–Ni^{2+} chelated pore to a 1 mM concentration of the neurotransmitters used in the experiments.

The sensitivity, reproducibility, and reversibility are also considered important features for the designing of a nanofluidic sensor. For this purpose, we have functionalized a second asymmetric pore with NTA–Ni^{2+} chelates, containing a higher number of active groups. Figures 3(A) and 3(B) illustrate the effect of the exposition to a 1 mM concentration of the same neurotransmitters as in Figures 2(C) and (D). The continuous lines in Figure 3(A) represent the results provided by the theoretical model. Again, the diameters of the pore were determined using the procedure described in section 2.7, and the surface charge density in each experiment was obtained from the best fitting at V = 1 V. As expected, the values of the measured currents in Figure 3(A) are significantly higher than those of Figure 2(C) due to the increase of the nanopore surface charge density. This fact results in a remarkable improvement of the specificity to Hm, as shown in Figure 3(B). Figures 3(C) and 3(D) show the changes observed in the I–V curves when the modified nanopore is exposed to electrolyte solutions having different Hm concentrations. Again, the continuous lines in Figure 3(C) correspond to the results provided by the theoretical model. The selective displacement of Ni^{2+} ions from the NTA moieties leads to a significant increase in the pore surface charges, in agreement with the surface charge densities calculated from the fittings. Figure 3(D) reveals a continuous increase in G(1 V) with the concentration of Hm. By increasing the analyte concentration, the number of metal-free NTA moieties increases

due to the displacement of the Ni^{2+} ion by Hm. This means that from an analytical point of view the system spans 5 orders of magnitude, which is a quite large dynamic range. At concentrations above 100 μM, further increase in the Hm concentration does not induce significant changes in G(1 V), suggesting the saturation of metal-free NTA moieties. Comparison of Figures 3(B) and 3(D) confirms quantitatively the remarkable specificity of the pore to Hm when compared to DA and the other analytes studied. Note that the exposure to only 500 nM Histamine gives the same effect that the addition of 1 mM Dopamine.

The sensing mechanism used in our experiments suggests that, given enough time, all the Ni^{2+} ions from the NTA moieties will be removed even in solutions with low Hm concentrations. Therefore, in order to produce a reliable sensor for Hm, the Ni^{2+} ions on the pore surface should equilibrate with Hm on a short timescale and diffusion of the Ni-Hm complex in and out the pore should occur at a lower rate. In that case, the chemical equilibrium of the displacement reaction follows a Langmuir isotherm and the surface charge densities calculated in Figure 4(C) must show an approximately sigmoidal dependence, see Reference [62]. The plot of Figure 4 confirms that this is indeed the case of our experiments, where the inflection point indicates the equilibrium constant of the displacement reaction.

Finally, we have evaluated also the reversibility of the nanopore-based sensing system. Figure 5 shows the variation of G(1 V) over different cycles of reversible binding and unbinding of the Ni^{2+} ion with the NTA moieties. When the Hm displaces the metal ions from the NTA–Ni^{2+} chelates, the exposed NTA moieties are available to Ni^{2+} ions. The reformation of NTA–Ni^{2+} complexes is evidenced by the drastic reduction in G(1 V) caused by the decrease in the charge density. Upon exposing to Hm solution, the initial conductance characteristics are restored because of the displacement of metal ion from the NTA moieties. The reversible changes in G(1 V) shown in Figure 5 suggest again that the surface charge density dictates the pore transport

properties, switching the nanopore from a high conducting state with NTA moieties to a low conducting state having NTA–Ni^{2+} chelates.

4. Conclusions

We have demonstrated the miniaturization of a nanofluidic device for the label-free specific detection of Hm neurotransmitter based on a metal ion displacement mechanism. To this end, pore walls were first decorated with NTA moieties through the covalent linkage of native carboxylic acid groups with BCML molecules. Then, the complexation of Ni^{2+} ion and NTA moieties led to the formation of NTA–Ni^{2+} chelates on the pore surface. This process altered the surface charge density and the pore conductance, as evidenced from the *I–V* curves before and after chemical treatment of the nanopore. The working principle of this nanofluidic sensor is based on the metal ion displacement from NTA–Ni^{2+} chelates by Hm. The proposed sensor has the ability to detect nanomolar concentrations of Hm in the working electrolyte because of the formation of stable Ni-Hm complexes. On the contrary, other neurotransmitters such as glycine, serotonin, gamma-aminobutyric acid, and dopamine could not induce such significant changes in the pore conductance due to their inability to displace and form stable complex with Ni^{2+} ion. The sensor exhibited high sensitivity, specificity, and reusability towards Hm detection. It has the potential to be clinically used for monitoring the concentration of biologically relevant neurotransmitters.

Acknowledgements

M.A., I.D., S.N. and W.E. acknowledge the funding from the Hessen State Ministry of Higher Education, Research and the Arts, Germany, under the LOEWE project iNAPO. P. R. and S. M.

acknowledge financial support by the Spanish Ministry of Economic Affairs and Competitiveness (MAT2015-65011-P) and FEDER. The authors are also thankful to Prof. C. Trautmann, Department of Materials Research from GSI, for support with irradiation experiments.

References

[1] E.R. Kandel, J.H. Schwartz, T.M. Jessell, S.A. Siegelbaum, Principles of Neural Science, 5th ed., McGraw-Hill, New York, 2012.
[2] R. Webster, Neurotransmitter Systems and Function: Overview, Neurotransmitters, Drugs and Brain Function, John Wiley & Sons, Ltd. 2002, pp. 1-32.
[3] F. András, K. Merétey, Histamine: an early messenger in inflammatory and immune reactions, Immunol. Today, 13 (1992) 154-156.
[4] J.-C. Schwartz, H. Pollard, T.T. Quach, Histamine as a Neurotransmitter in Mammalian Brain: Neurochemical Evidence, J. Neurochem., 35 (1980) 26-33.
[5] M.V. White, The role of histamine in allergic diseases, J. Allergy Clin. Immunol., 86 (1990) 599-605.
[6] E.W. Gelfand, Role of histamine in the pathophysiology of asthma: immunomodulatory and anti-inflammatory activities of H1-receptor antagonists, Am. J. Med., 113 (2002) 2-7.
[7] T. Pradhan, H.S. Jung, J.H. Jang, T.W. Kim, C. Kang, J.S. Kim, Chemical sensing of neurotransmitters, Chem. Soc. Rev., 43 (2014) 4684-4713.
[8] L. Maintz, N. Novak, Histamine and histamine intolerance, Am. J. Clin. Nutr., 85 (2007) 1185-1196.
[9] L. Lehane, J. Olley, Histamine fish poisoning revisited, Int. J. Food Microbiol., 58 (2000) 1-37.
[10] S.L. Taylor, J.E. Stratton, J.A. Nordlee, Histamine Poisoning (Scombroid Fish Poisoning): An Allergy-Like Intoxication, J. Toxicol. Clin. Toxicol., 27 (1989) 225-240.
[11] F.R. Antoine, C.-I. Wei, W.S. Otwell, C.A. Sims, R.C. Littell, A.D. Hogle, M.R. Marshall, Gas Chromatographic Analysis of Histamine in Mahi-mahi (Coryphaena hippurus), J. Agric. Food Chem., 50 (2002) 4754-4759.
[12] N. Garcia-Villar, J. Saurina, S. Hernandez-Cassou, Determination of histamine in wines with an on-line pre-column flow derivatization system coupled to high performance liquid chromatography, Analyst, 130 (2005) 1286-1290.
[13] T. Yoshitake, F. Ichinose, H. Yoshida, K.-I. Todoroki, J. Kehr, O. Inoue, H. Nohta, M. Yamaguchi, A sensitive and selective determination method of histamine by HPLC with intramolecular excimer-forming derivatization and fluorescence detection, Biomed. Chromatogr., 17 (2003) 509-516.
[14] L.-Y. Zhang, M.-X. Sun, Determination of histamine and histidine by capillary zone electrophoresis with pre-column naphthalene-2,3-dicarboxaldehyde derivatization and fluorescence detection, J. Chromatogr. A, 1040 (2004) 133-140.
[15] N. García-Villar, J. Saurina, S. Hernández-Cassou, Capillary electrophoresis determination of biogenic amines by field-amplified sample stacking and in-capillary derivatization, Electrophoresis, 27 (2006) 474-483.
[16] Q. Peng, J. He, C. Jiang, A new spectrofluorimetric method for determination of trace amounts histamine in human urine and serum, Luminescence, 24 (2009) 135-139.
[17] D. Seto, N. Soh, K. Nakano, T. Imato, Selective fluorescence detection of histamine based on ligand exchange mechanism and its application to biomonitoring, Anal. Biochem., 404 (2010) 135-139.
[18] D. Seto, N. Soh, K. Nakano, T. Imato, An amphiphilic fluorescent probe for the visualization of histamine in living cells, Bioorg. Med. Chem. Lett., 20 (2010) 6708-6711.
[19] O. Niwa, R. Kurita, K. Hayashi, T. Horiuchi, K. Torimitsu, K. Maeyama, K. Tanizawa, Continuous measurement of histamine from rat basophilic leukemia cells (RBL-2H3) with an on-line sensor using histamine oxidase, Sens. Actuators B., 67 (2000) 43-51.
[20] Y. Li, M. Kobayashi, K. Furui, N. Soh, K. Nakano, T. Imato, Surface plasmon resonance immunosensor for histamine based on an indirect competitive immunoreaction, Anal. Chim. Acta, 576 (2006) 77-83.

[21] Y. Oshikawa, K. Furuta, S. Tanaka, A. Ojida, Cell Surface-Anchored Fluorescent Probe Capable of Real-Time Imaging of Single Mast Cell Degranulation Based on Histamine-Induced Coordination Displacement, Anal. Chem., 88 (2016) 1526-1529.
[22] C. Dekker, Solid-state nanopores, Nat. Nanotechnol., 2 (2007) 209-215.
[23] R.E. Gyurcsanyi, Chemically-modified nanopores for sensing, Trends Anal. Chem., 27 (2008) 627-639.
[24] K. Healy, B. Schiedt, A.P. Morrison, Solid-state nanopore technologies for nanopore-based DNA analysis, Nanomedicine, 2 (2007) 875-897.
[25] S. Howorka, Z. Siwy, Nanopore analytics: sensing of single molecules, Chem. Soc. Rev., 38 (2009) 2360-2384.
[26] J.J. Kasianowicz, J.W.F. Robertson, E.R. Chan, J.E. Reiner, V.M. Stanford, Nanoscopic porous sensors, Ann. Rev. Anal. Chem., 1 (2008) 737-766.
[27] Z.S. Siwy, S. Howorka, Engineered voltage-responsive nanopores, Chem. Soc. Rev., 39 (2010) 1115-1132.
[28] M. Ali, S. Nasir, Q.H. Nguyen, J.K. Sahoo, M.N. Tahir, W. Tremel, W. Ensinger, Metal Ion Affinity-based Biomolecular Recognition and Conjugation inside Synthetic Polymer Nanopores Modified with Iron-Terpyridine Complexes, J. Am. Chem. Soc., 133 (2011) 17307-17314.
[29] M. Ali, S. Nasir, P. Ramirez, J. Cervera, S. Mafe, W. Ensinger, Carbohydrate-Mediated Biomolecular Recognition and Gating of Synthetic Ion Channels, J. Phys. Chem. C, 117 (2013) 18234-18242.
[30] M. Ali, P. Ramirez, M.N. Tahir, S. Mafe, Z. Siwy, R. Neumann, W. Tremel, W. Ensinger, Biomolecular conjugation inside synthetic polymer nanopores via glycoprotein-lectin interactions, Nanoscale, 3 (2011) 1894-1903.
[31] M. Ali, B. Schiedt, R. Neumann, W. Ensinger, Biosensing with Functionalized Single Asymmetric Polymer Nanochannels, Macromol. Biosci., 10 (2010) 28-32.
[32] Z. Siwy, L. Trofin, P. Kohli, L.A. Baker, C. Trautmann, C.R. Martin, Protein biosensors based on biofunctionalized conical gold nanotubes, J. Am. Chem. Soc., 127 (2005) 5000-5001.
[33] M.N. Tahir, M. Ali, R. Andre, W.E.G. Muller, H.-C. Schroder, W. Tremel, W. Ensinger, Silicatein conjugation inside nanoconfined geometries through immobilized NTA-Ni(ii) chelates, Chem. Commun., 49 (2013) 2210-2212.
[34] I. Vlassiouk, T.R. Kozel, Z.S. Siwy, Biosensing with Nanofluidic Diodes, J. Am. Chem. Soc., 131 (2009) 8211-8220.
[35] M. Lepoitevin, M. Bechelany, E. Balanzat, J.-M. Janot, S. Balme, Non-Fluorescence label protein sensing with track-etched nanopore decorated by avidin/biotin system, Electrochim. Acta, 211 (2016) 611-618.
[36] M. Ali, S. Nasir, P. Ramirez, J. Cervera, S. Mafe, W. Ensinger, Calcium Binding and Ionic Conduction in Single Conical Nanopores with Polyacid Chains: Model and Experiments, ACS Nano, 6 (2012) 9247-9257.
[37] C. Han, H. Su, Z. Sun, L. Wen, D. Tian, K. Xu, J. Hu, A. Wang, H. Li, L. Jiang, Biomimetic Ion Nanochannels as a Highly Selective Sequential Sensor for Zinc Ions Followed by Phosphate Anions, Chem. Eur. J., 19 (2013) 9388-9395.
[38] X. Hou, W. Guo, F. Xia, F.Q. Nie, H. Dong, Y. Tian, L.P. Wen, L. Wang, L.X. Cao, Y. Yang, J.M. Xue, Y.L. Song, Y.G. Wang, D.S. Liu, L. Jiang, A Biomimetic Potassium Responsive Nanochannel: G-Quadruplex DNA Conformational Switching in a Synthetic Nanopore, J. Am. Chem. Soc., 131 (2009) 7800-7805.
[39] Q. Liu, K. Xiao, L. Wen, H. Lu, Y. Liu, X.-Y. Kong, G. Xie, Z. Zhang, Z. Bo, L. Jiang, Engineered Ionic Gates for Ion Conduction Based on Sodium and Potassium Activated Nanochannels, J. Am. Chem. Soc., 137 (2015) 11976-11983.
[40] Z. Sun, F. Zhang, X. Zhang, D. Tian, L. Jiang, H. Li, Chiral recognition of Arg based on label-free PET nanochannel, Chem. Commun., 51 (2015) 4823-4826.
[41] Y. Tian, X. Hou, L. Wen, W. Guo, Y. Song, H. Sun, Y. Wang, L. Jiang, D. Zhu, A biomimetic zinc activated ion channel, Chem. Commun., 46 (2010) 1682-1684.

[42] M. Ali, I. Ahmed, P. Ramirez, S. Nasir, J. Cervera, C.M. Niemeyer, W. Ensinger, Fluoride-induced modulation of ionic transport in asymmetric nanopores functionalized with "caged" fluorescein moieties, Nanoscale, 8 (2016) 8583-8590.
[43] Q. Liu, K. Xiao, L. Wen, Y. Dong, G. Xie, Z. Zhang, Z. Bo, L. Jiang, A Fluoride-Driven Ionic Gate Based on a 4-Aminophenylboronic Acid-Functionalized Asymmetric Single Nanochannel, ACS Nano, 8 (2014) 12292-12299.
[44] G. Nie, Y. Sun, F. Zhang, M. Song, D. Tian, L. Jiang, H. Li, Fluoride responsive single nanochannel: click fabrication and highly selective sensing in aqueous solution, Chem. Sci., 6 (2015) 5859-5865.
[45] M. Ali, S. Nasir, W. Ensinger, Stereoselective detection of amino acids with protein-modified single asymmetric nanopores, Electrochim Acta, 215 (2016) 231-237.
[46] A.J. Boersma, H. Bayley, Continuous Stochastic Detection of Amino Acid Enantiomers with a Protein Nanopore, Angew. Chem. Int. Ed., 51 (2012) 9606-9609.
[47] C.P. Han, X. Hou, H.C. Zhang, W. Guo, H.B. Li, L. Jiang, Enantioselective Recognition in Biomimetic Single Artificial Nanochannels, J. Am. Chem. Soc., 133 (2011) 7644-7647.
[48] S.B. Lee, D.T. Mitchell, L. Trofin, T.K. Nevanen, H. Soderlund, C.R. Martin, Antibody-based bio-nanotube membranes for enantiomeric drug separations, Science, 296 (2002) 2198-2200.
[49] G. Xie, W. Tian, L. Wen, K. Xiao, Z. Zhang, Q. Liu, G. Hou, P. Li, Y. Tian, L. Jiang, Chiral recognition of l-tryptophan with beta-cyclodextrin-modified biomimetic single nanochannel, Chem. Commun., 51 (2015) 3135-3138.
[50] M. Ali, I. Ahmed, P. Ramirez, S. Nasir, C.M. Niemeyer, S. Mafe, W. Ensinger, Label-Free Pyrophosphate Recognition with Functionalized Asymmetric Nanopores, Small, 12 (2016) 2014-2021.
[51] P.Y. Apel, Y.E. Korchev, Z. Siwy, R. Spohr, M. Yoshida, Diode-Like Single-Ion Track Membrane Prepared by Electro-Stopping, Nucl. Instrum. Methods Phys. Res., Sect. B, 184 (2001) 337-346.
[52] M. Ali, P. Ramirez, S. Mafe, R. Neumann, W. Ensinger, A pH-Tunable Nanofluidic Diode with a Broad Range of Rectifying Properties, ACS Nano, 3 (2009) 603-608.
[53] J. Cervera, B. Schiedt, R. Neumann, S. Mafe, P. Ramirez, Ionic Conduction, Rectification, and Selectivity in Single Conical Nanopores, J. Chem. Phys., 124 (2006) 104706.
[54] J. Cervera, B. Schiedt, P. Ramirez, A Poisson/Nernst-Planck model for ionic transport through synthetic conical nanopores, Europhys. Lett., 71 (2005) 35-41.
[55] T.A. Zangle, A. Mani, J.G. Santiago, Theory and experiments of concentration polarization and ion focusing at microchannel and nanochannel interfaces, Chem. Soc. Rev., 39 (2010) 1014-1035.
[56] P. Ramirez, P.Y. Apel, J. Cervera, S. Mafe, Pore Structure and Function of Synthetic Nanopores with Fixed Charges: Tip Shape and Rectification Properties, Nanotechnology, 19 (2008) 315707.
[57] P. Ramirez, V. Gomez, J. Cervera, B. Schiedt, S. Mafe, Ion transport and selectivity in nanopores with spatially inhomogeneous fixed charge distributions, J. Chem. Phys., 126 (2007) 194703.
[58] Z.S. Siwy, Ion-Current Rectification in Nanopores and Nanotubes with Broken Symmetry, Adv. Funct. Mater., 16 (2006) 735-746.
[59] N.A. Kostromina, V.P. Tikhonov, PMR study of the complex formation of L-histidine with nickel(II), Theor. Exp. Chem., 16 (1981) 396-402.
[60] B. Rao, H.B. Mathur, Thermodynamics of the interaction of transition metal ions with histamine, J. Inorg. Nucl. Chem., 33 (1971) 809-816.
[61] P. Drożdżewski, E. Kordon, Isotopic labelling studies on far-infrared spectra of nickel–histamine complexes, Spectrochim. Acta A, 56 (2000) 2459-2464.
[62] M. Tagliazucchi, I. Szleifer, How Does Confinement Change Ligand–Receptor Binding Equilibrium? Protein Binding in Nanopores and Nanochannels, J. Am. Chem. Soc., 137 (2015) 12539-12551.

Figures and Captions

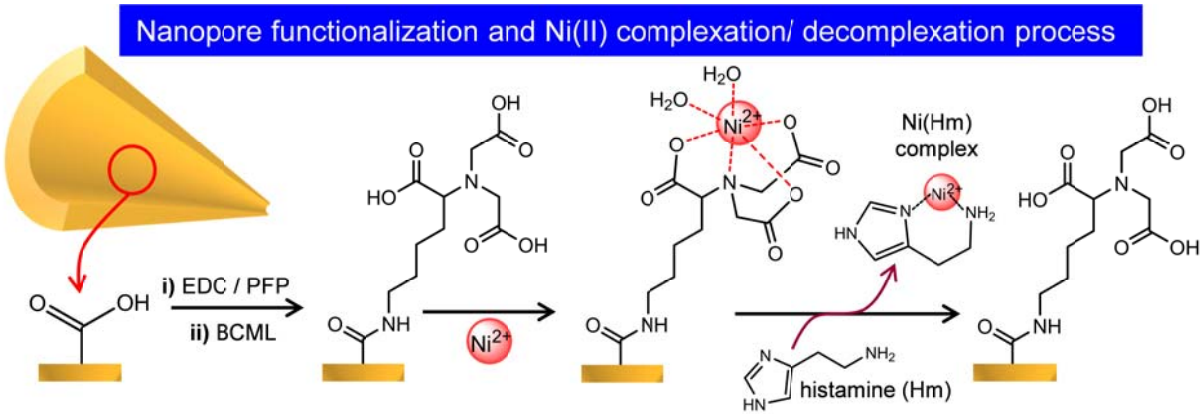

Figure 1. Reaction scheme representing the chemical functionalization of BCML chains having NTA moiety, the Ni(II)–NTA complexation, and the regeneration of NTA group by the removal of Ni^{2+} ions on exposure to Hm solution.

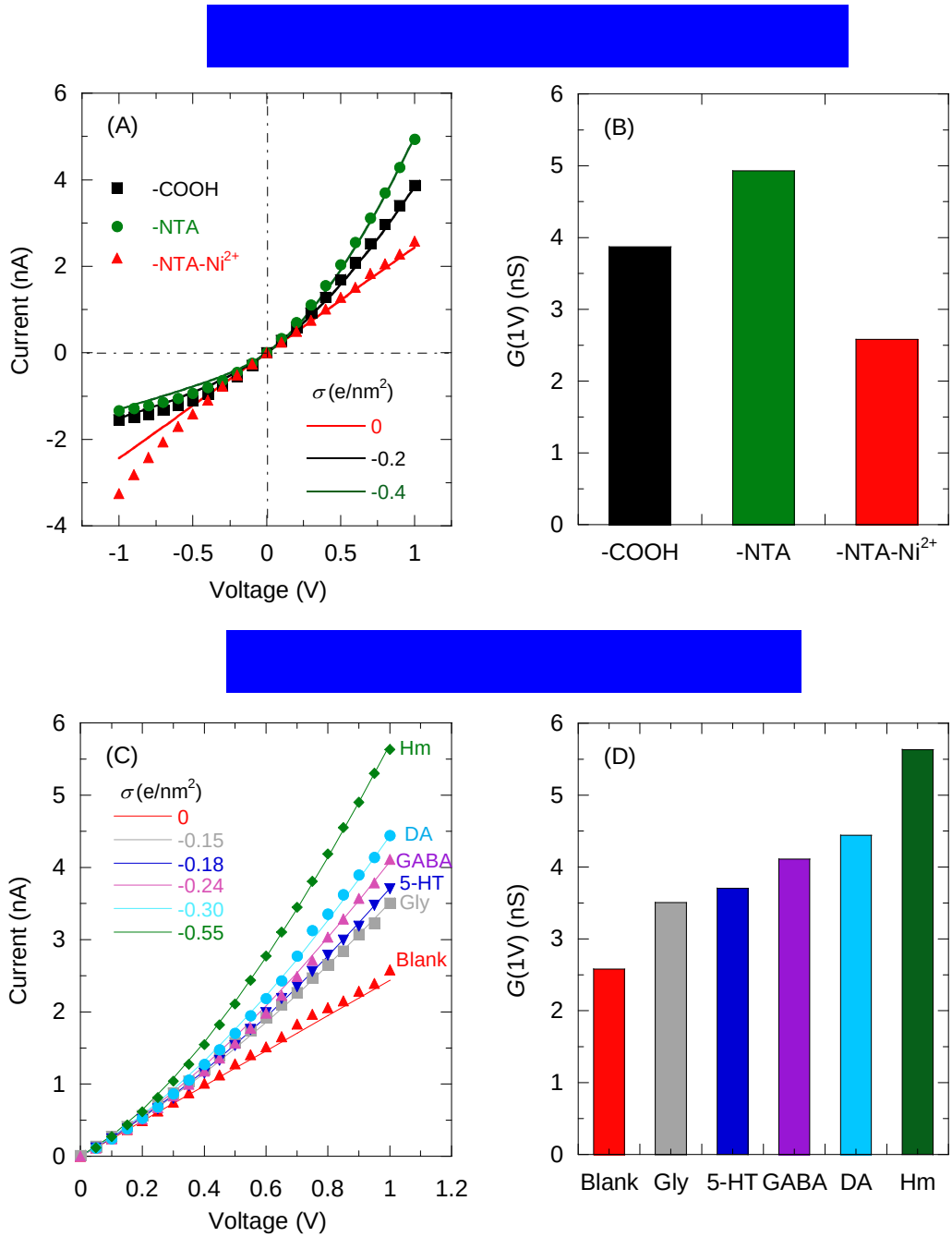

Figure 2. (A) *I–V* curves of a single conical nanopore (*d* = 35 nm, *D* = 700 nm) bearing carboxylate groups (as-prepared pore), NTA moieties (modified pore) and NTA-Ni^{2+} chelates. (B) Changes in the conductance measured at 1 V. (C) *I–V* curves of NTA-Ni^{2+} chelated pore prior to (blank) and after exposure to different analytes at concentration 1mM in the electrolyte solution: glycine (Gly), serotonin (5-HT), gamma-aminobutyric acid (GABA), dopamine (DA) and histamine (Hm). (D) Changes in the conductance measured at 1 V. The continuous lines in (A) and (C) are the results of a 1D PNP model.

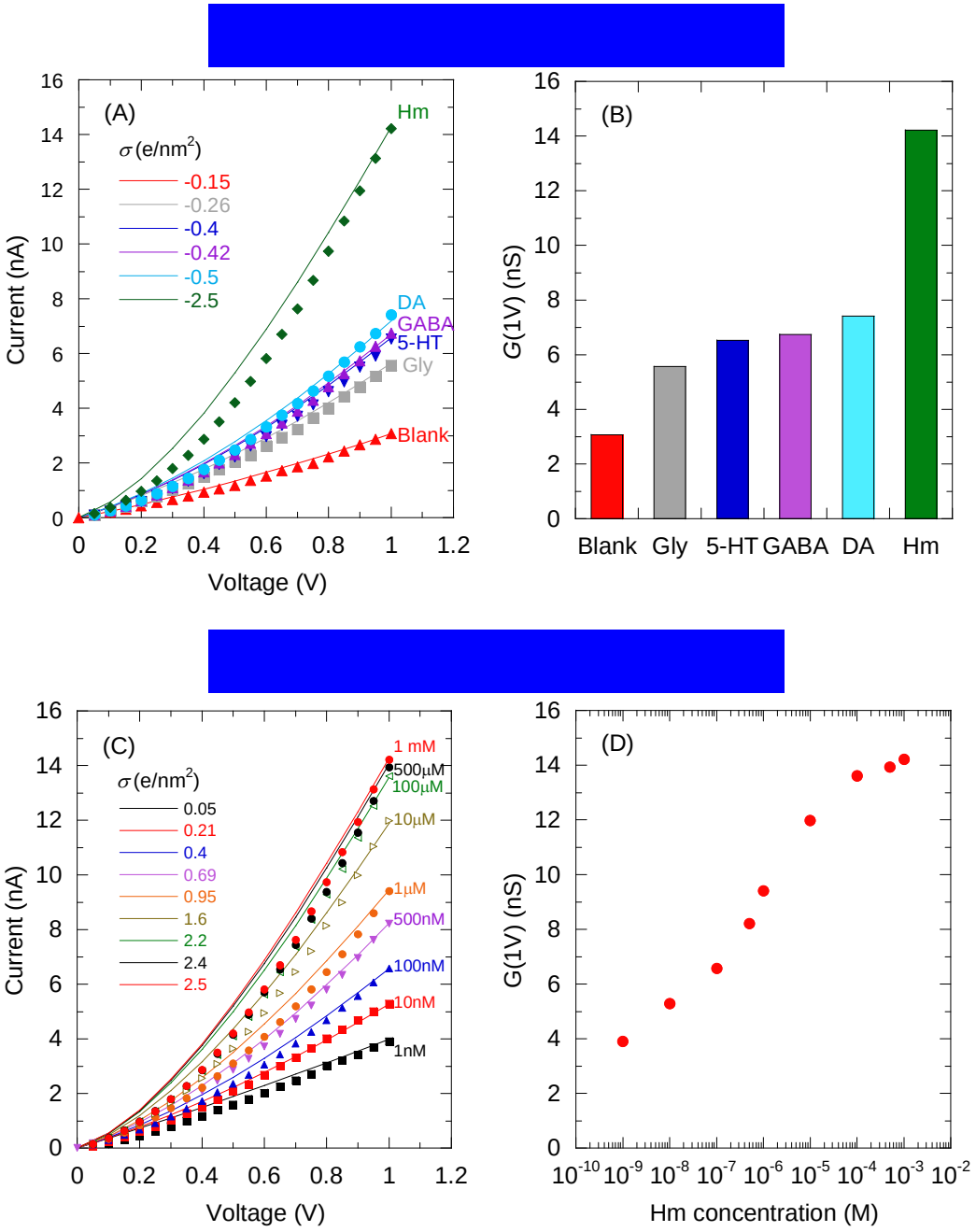

Figure 3. (A) *I–V* curves of NTA-Ni^{2+} chelated pore (*d* = 45 nm; *D* = 800 nm) prior to (blank) and after exposure to different analytes at concentration 1mM in the electrolyte solution: glycine (Gly), serotonin (5-HT), gamma-aminobutyric acid (GABA), dopamine (DA) and histamine (Hm). (B) Changes in the conductance measured at 1 V. (C) *I–V* curves upon exposure to different concentrations of Hm. (D) Changes in the conductance measured at 1 V. The continuous lines in (A) and (C) are the results of a 1D PNP model.

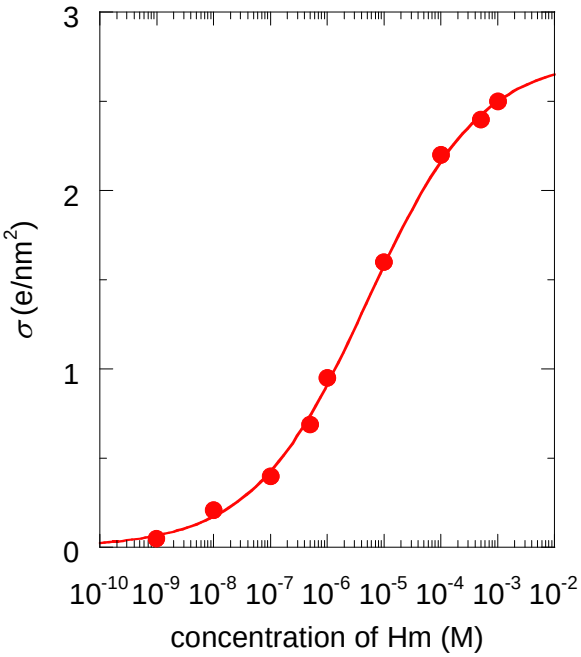

Figure 4. Surface charge density obtained from the fittings of theory to experiments as a function of the concentration of Hm. The sigmoid dependence indicates that the Ni ions of the pore surface equilibrate with Hm on a short timescale and that diffusion of the Ni-Hm complex in and out the pore occurs at slower rate.

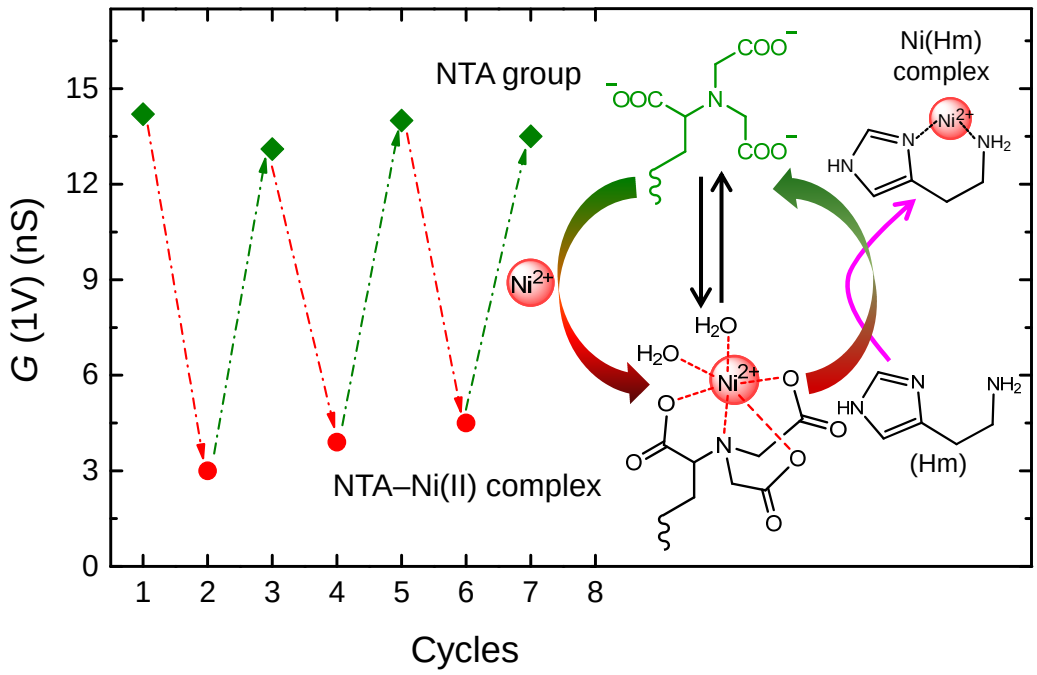

Figure 5. Different cycles representing the changes obtained in *G*(1 V) as a result of the reversible complexation/decomplexation of Ni(II) with the NTA moieties.